eLIFE
elifesciences.org

# Figures and figure supplements

Cryo-EM visualization of the ribosome in termination complex with apo-RF3 and RF1

**Jesper Pallesen, et al.**

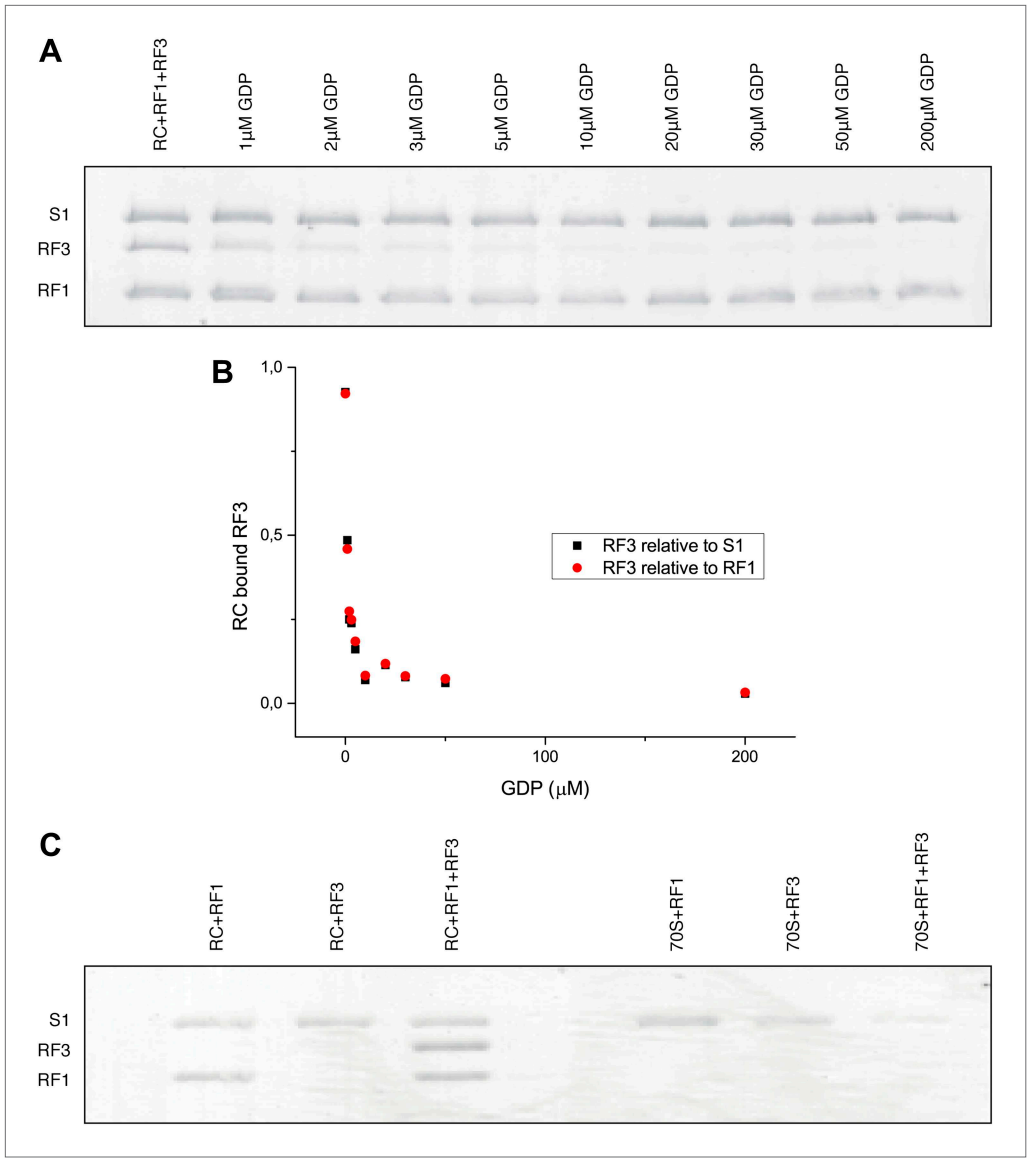


**Figure 1**. Occupancy of RF1 and RF3 in the RC–RF1•RF3 complex and the effect of extra added GDP. (**A**) Titrating GDP into a release complex (RC) programmed with Met-stop mRNA, and containing fMet-tRNA$^{fMet}$ (in the P site), RF1 and RF3. The intensity of the band corresponding to RF3 decreased gradually to zero with increasing GDP concentration, but the S1 and RF1 intensities remained unaltered. (**B**) RF3 band intensity relative to S1 and RF1 plotted vs GDP concentration. (**C**) RC (lanes 1–3) and naked 70S ribosome (lanes 4–6) were incubated with either RF1 alone, RF3 alone or with both RF1 and RF3 as control experiments. RF3 could be detectably bound only to RC—and not to 70S—, when RF1 was present in the complex (lane 3). This confirms that the RF3 bands seen in the gel—in both panels **A** and **C**—indeed arise from functional complex formation.

DOI: 10.7554/eLife.00411.003

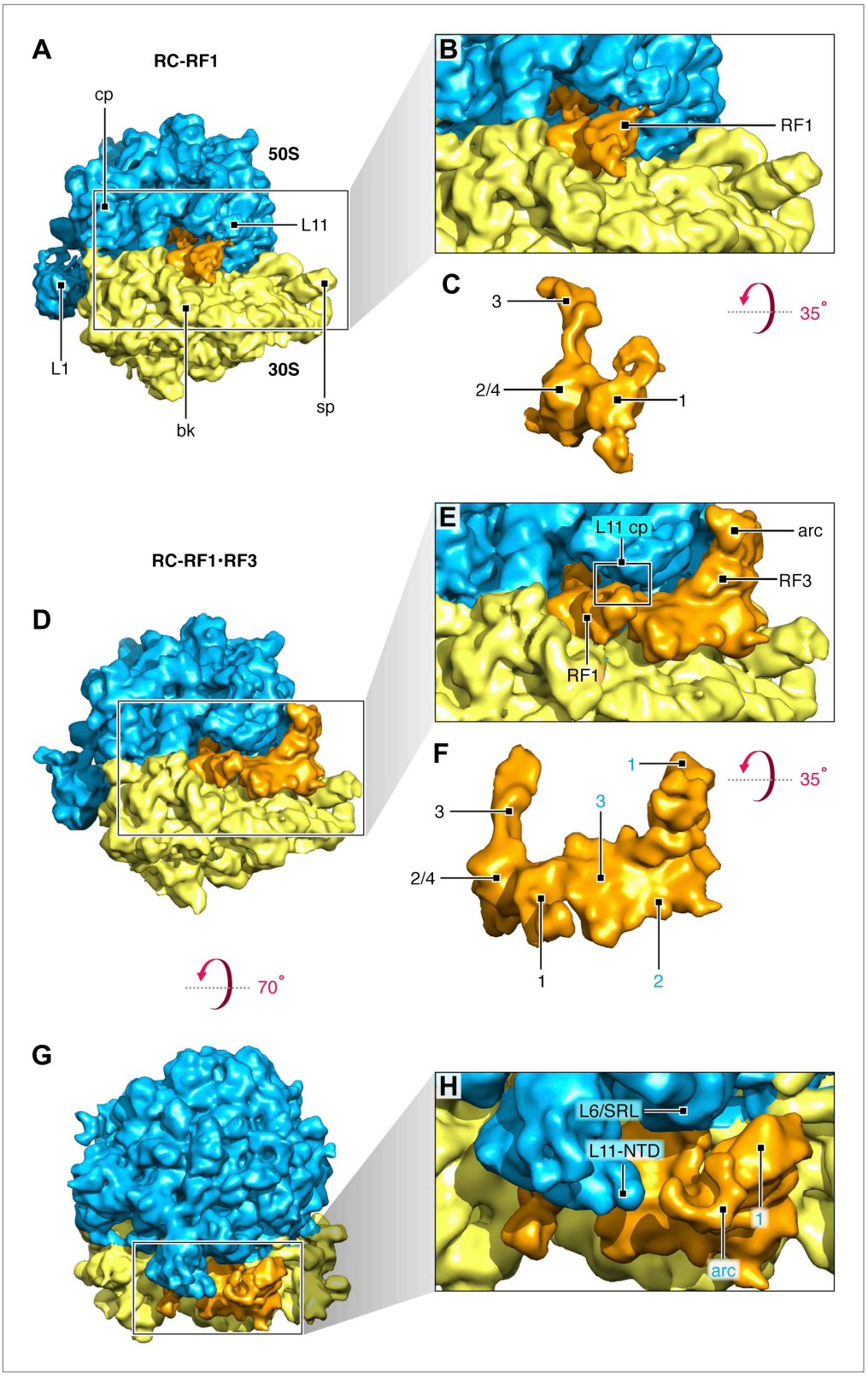


**Figure 2**. Termination complexes in association with RF1 alone and with both RF1 and apo-RF3. (**A**) RC-RF1 (resolution 8.4 Å). (**B**) Close-up of RF1 in the map. (**C**) RF1 density from (**B**). Domains 1, 2/4 and 3 of RF1 are labeled. (**D**) RC–RF1•RF3 (resolution 9.7 Å). (**E**) Close-up of RF1and apo-RF3 in the map. RF1 contacts both L11—L11 contact

*Figure 2. Continued on next page*

*Figure 2. Continued*

point is labeled 'L11 cp'— and apo-RF3. (**F**) Density of RF1 and RF3 from (**E**): RF1 domains labeled in black and RF3 domains 1, 2 and 3 in blue. (**G**)–(**H**) In the RC–RF1•RF3 complex, apo-RF3 does not interact with L11 or L6/SRL. Labels: 30S: small ribosomal subunit (yellow), 50S: large ribosomal subunit (blue), cp: central protuberance, L11: ribosomal protein L11, sp: spur, bk: beak, L1: L1 stalk, RF1: release factor 1, RF3: release factor 3, L6/SRL: position of ribosomal protein L6 and the sarcin/ricin loop, L11-NTD: ribosomal protein L11 N-terminal domain, arc: arc-like density. Density maps obtained from the total data set and of the RC-class not occupied by RF1 or RF3 are presented in ***Figure 2—figure supplement 1*** and ***Figure 2—figure supplement 2***, respectively. Additional panels of isolated RF1- and RF1, apo-RF3-densities are presented in ***Figure 2—figure supplement 3***. FSC curves for resolution assessment of all density maps obtained can be found in ***Figure 2—figure supplement 4***.

DOI: 10.7554/eLife.00411.004

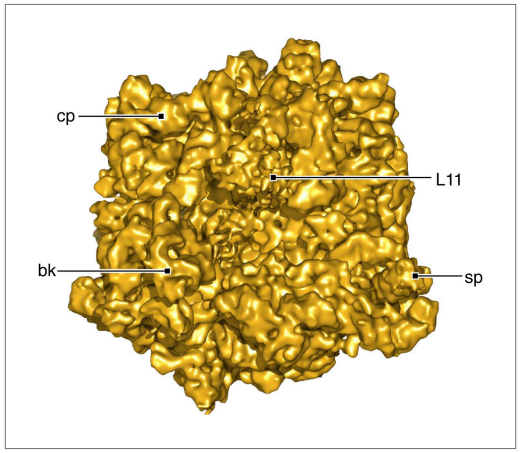


**Figure 2—figure supplement 1**. Density map resulting from refinement of the full data set. Map is displayed at a resolution of 6.3 Å in accordance with a Fourier shell correlation (FSC) of 0.14 between half sets. Labels same as in ***Figure 2***.

DOI: 10.7554/eLife.00411.005

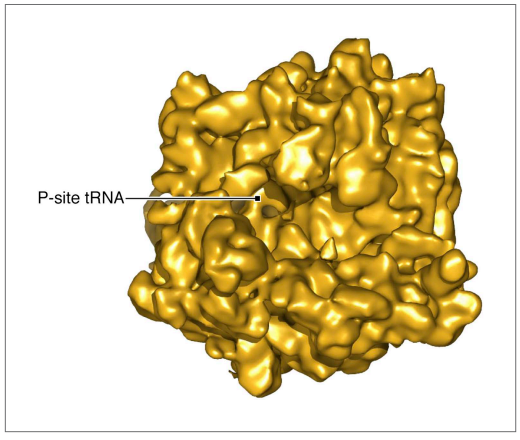


**Figure 2—figure supplement 2**. Density map resulting from refinement of the 'RC' class identified in our classification. The map shows the ribosome occupied with a P-site tRNA but no release factors.

DOI: 10.7554/eLife.00411.006

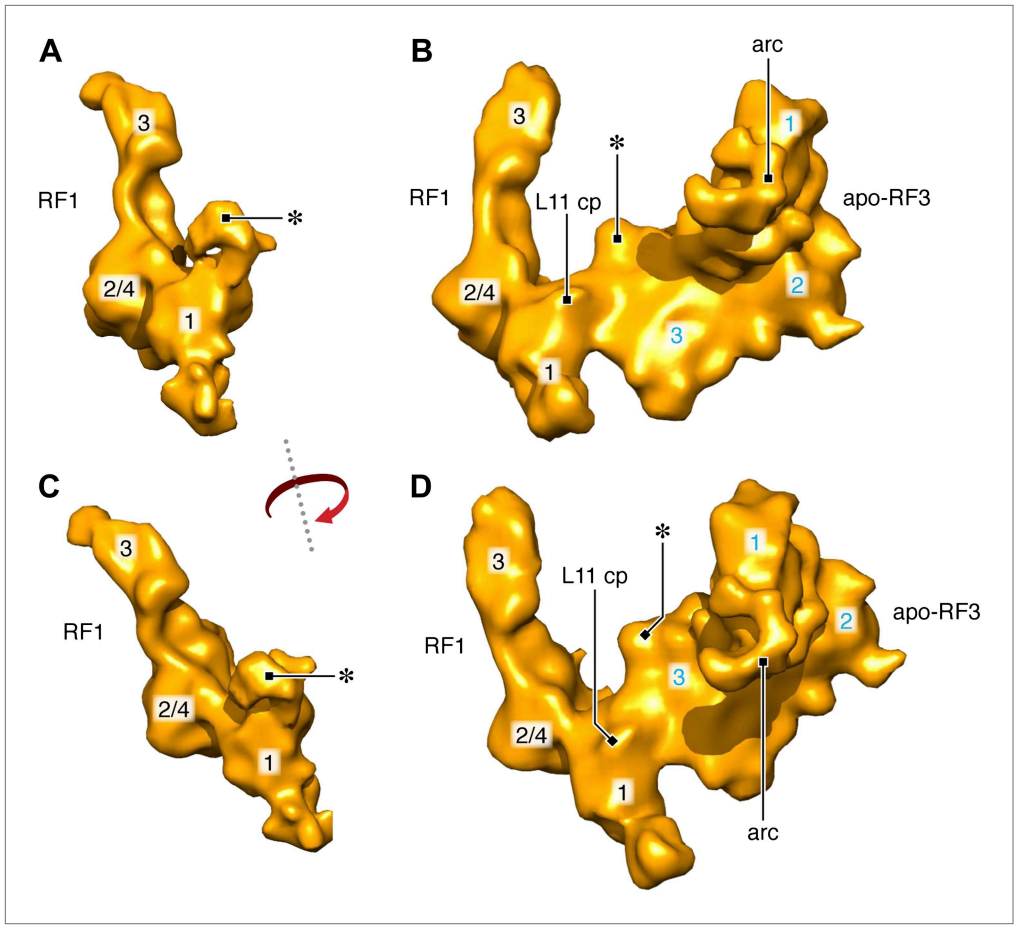


**Figure 2—figure supplement 3**. Segmented RF1 and RF1, apo-RF3 densities. (**A**), (**C**) Segmented RF1 density from RC-RF1, compared to the segmented, combined RF1, apo-RF3 density from RC-RF1•RF3 (**B**), (**D**). Density marked by asterisk in (**A**) and (**C**) is no longer present in (**B**) and (**D**); instead redistributed density is observed in RF1 domain 1 (asterisk in [**B**] and [**D**]) upon apo-RF3 binding. The arc of RF3 is labeled in all panels featuring RF3. L11 cp marks the point of contact between L11 and RF3 in the RC-RF1•RF3 map. RF3 domains labeled in blue; RF1 domains in black.

DOI: 10.7554/eLife.00411.007

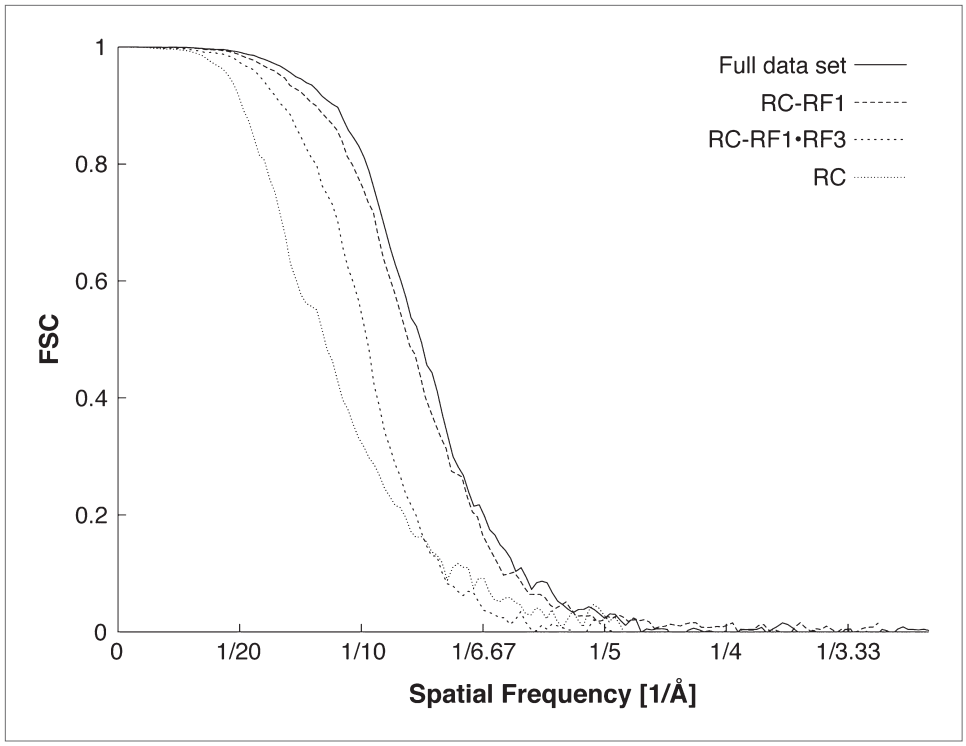


**Figure 2—figure supplement 4**. FSC curves for density maps obtained from total data, RC, RC-RF1 and RC-RF1•RF3. Resolutions, determined using the FSC = 0.5 cutoff criterion, are 8.0 Å (full data set), 8.4 Å (RC-RF1), 9.7 Å (RC-RF1•RF3) and 11.8 Å (RC).

DOI: 10.7554/eLife.00411.008

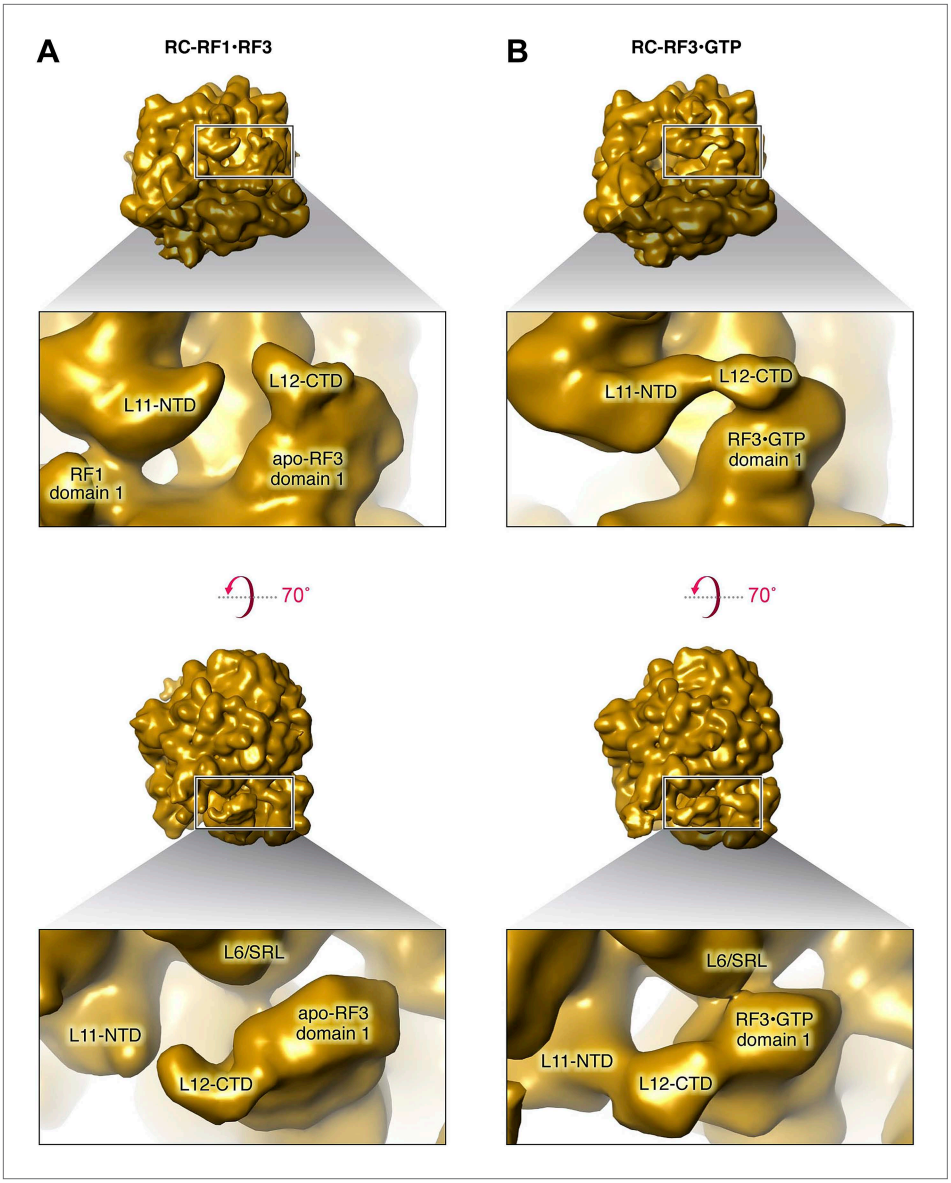


**Figure 3**. Comparison of L11, L6/SRL, arc (L12-CTD) and apo-RF3 in RC-RF1•RF3 and RC-RF3 maps. (**A**) Apo-RF3 is observed in contact with L12-CTD (arc) but L12-CTD is not in contact with L11-NTD. Apo-RF3 domain 1 is not in contact with L6/SRL. In contrast (**B**), RF3•GTP is observed in contact with L6/SRL and in this map (RC-RF3•GTP), L12-CTD is in contact with both RF3 domain 1 and L11-NTD. Both maps are displayed at the resolution of the latter—16 Å—for direct comparison; unsegmented maps were chosen to avoid artifacts on the edges of protein densities and, hence, to present a correct analysis of the interactions occurring.

DOI: 10.7554/eLife.00411.009

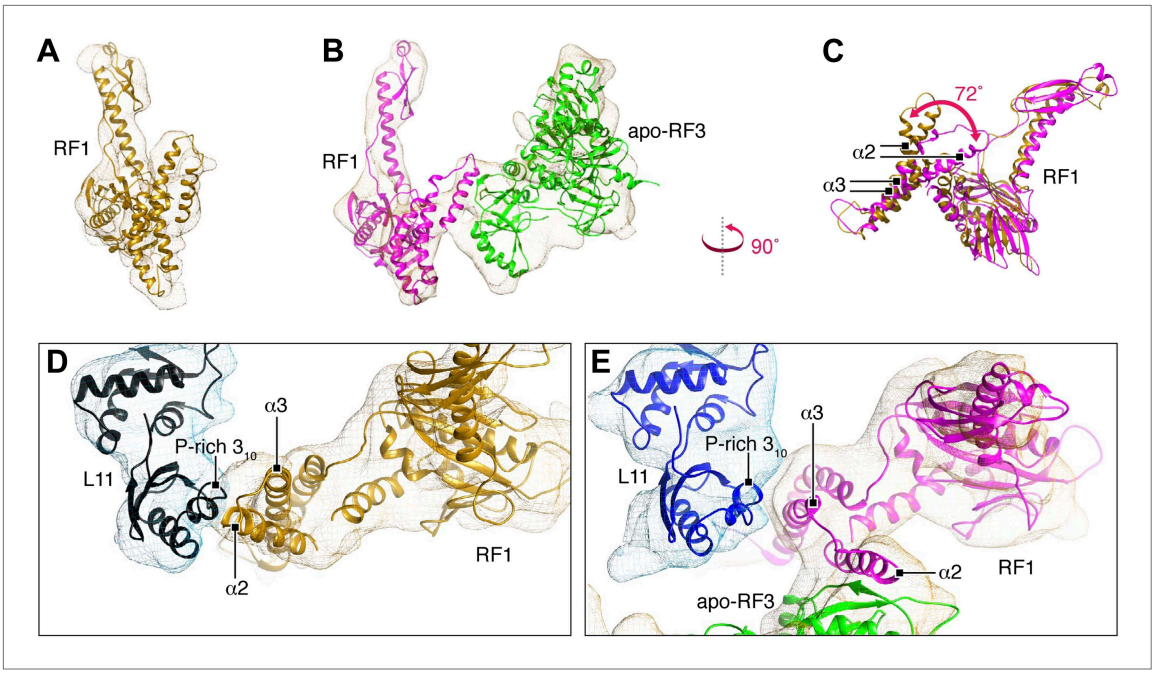


**Figure 4**. Flexible fitting by MDFF focusing on RF1 conformation and interactions. (**A**)–(**C**) Comparison of *E. coli* RF1 conformations after MDFF. (**A**) RF1 in RC-RF1. (**B**) RF1 (and RF3) in RC-RF1•RF3. (**C**) Superimposition of RF1 from (**A**) and (**B**). Arrow in (**C**) denotes the conformational change of domain 1. (**D**) In the RC-RF1 complex, RF1 interacts through helices α2 and α3 with the P-rich $3_{10}$-helix in the L11-NTD. (**E**) In the RC-RF1•RF3 complex α3 (RF1) interacts with the $3_{10}$-helix (L11-NTD), while α2 (RF1) interacts with RF3. α2 and α3 denote helices α2 and α3 in domain 1 of RF1; P-rich $3_{10}$ denotes the P-rich $3_{10}$ helix in L11-NTD. Root mean square deviation and cross correlation coefficient plots for our MD flexible fitting are presented in ***Figure 4—figure supplement 1***.

DOI: 10.7554/eLife.00411.010

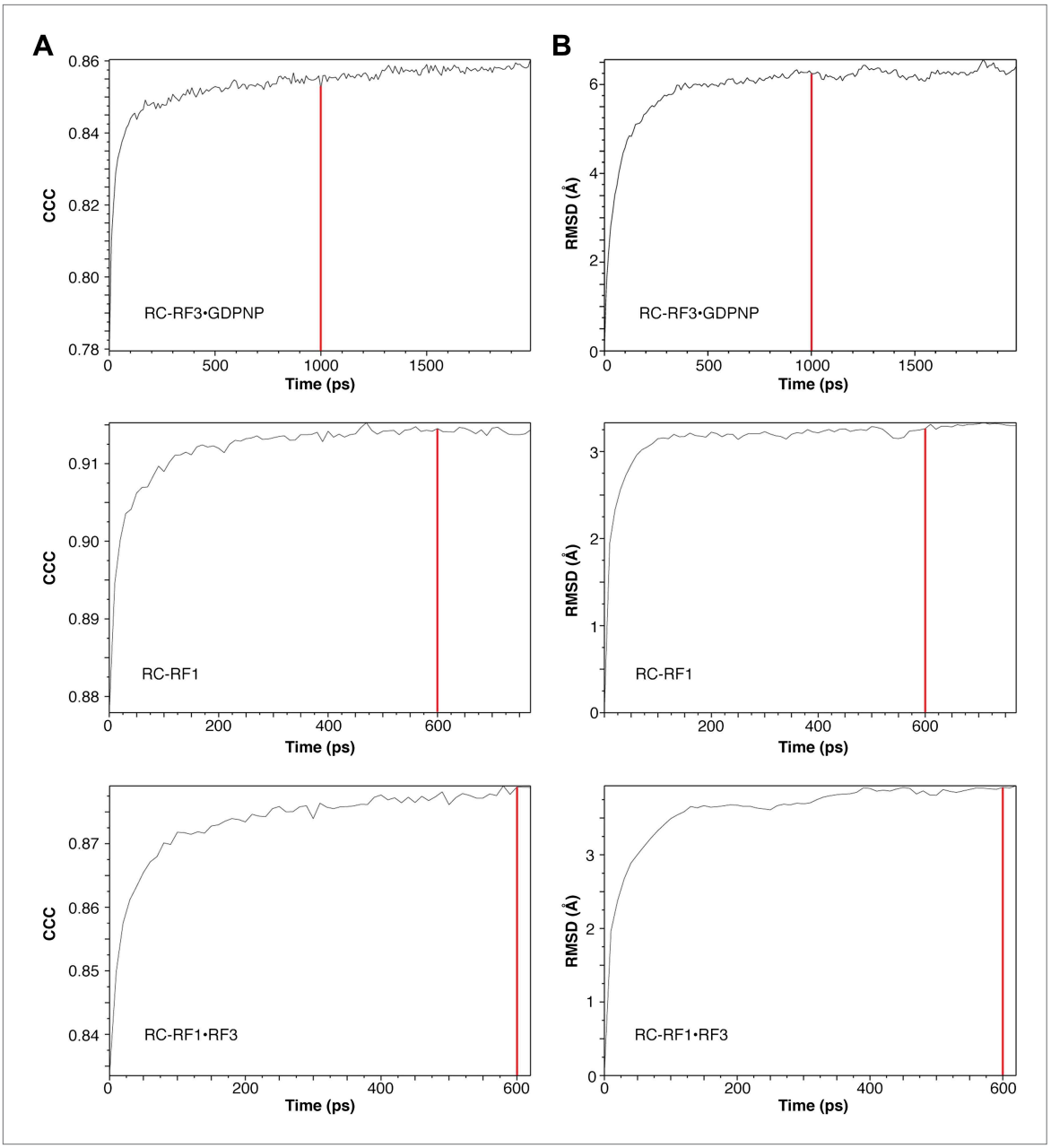


**Figure 4—figure supplement 1**. RMSD and CCC values for MD flexible fitting. (**A**) Root mean square deviation (RMSD) over the course of MD flexible fitting between model in current frame and initial model in the three systems. (**B**) Cross-correlation coefficients (CCC) over the course of MD flexible fitting between models and density maps. Red lines indicate the time points at which frames (models) were selected for presentation in this study.
DOI: 10.7554/eLife.00411.011

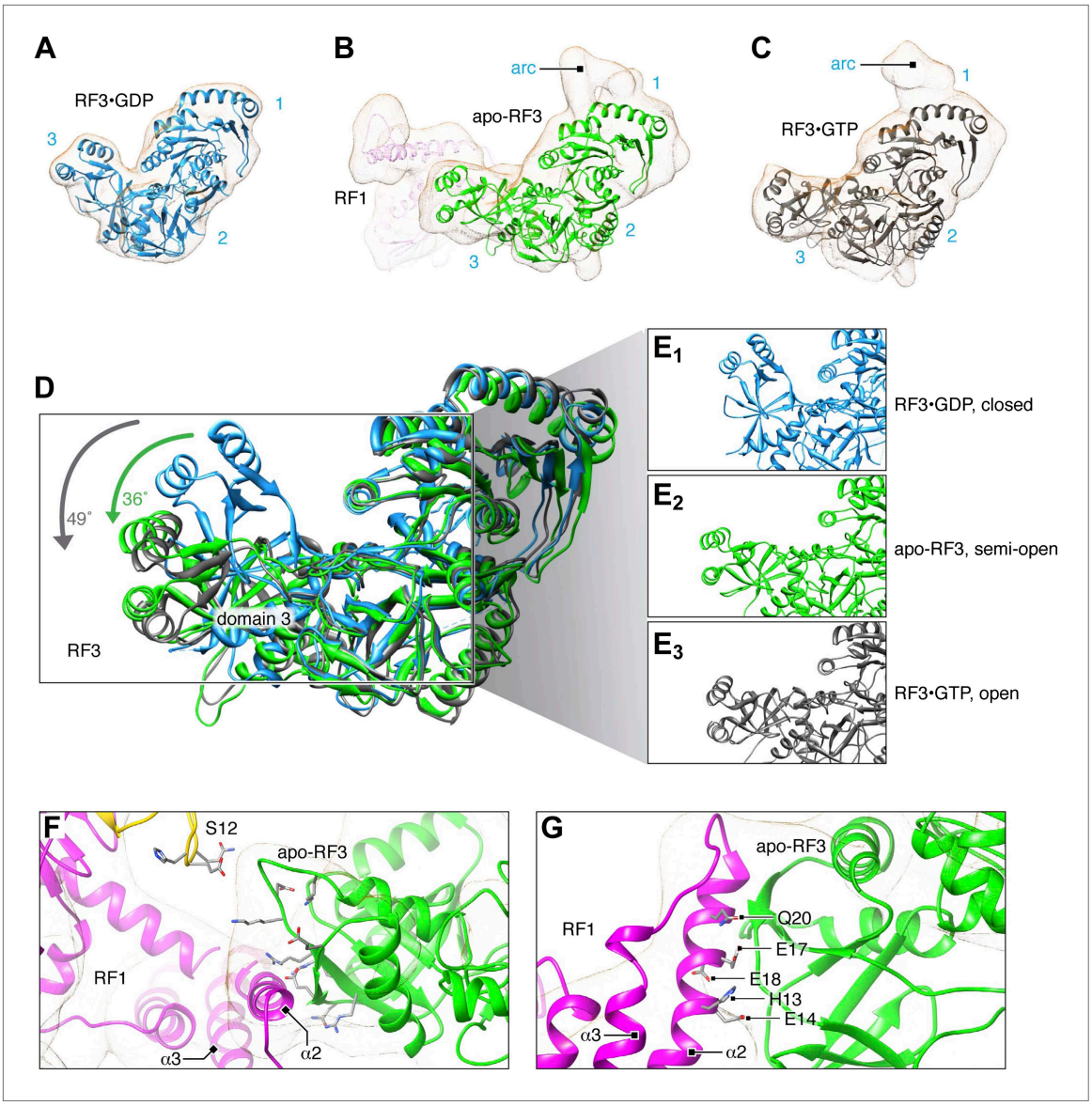


**Figure 5**. Flexible fitting by MDFF focusing on RF3 conformation and interaction with RF1. (**A**)–(**C**) Comparison of *E. coli* RF3 conformations after MDFF. (**A**) Crystal structure of free RF3•GDP displayed in its simulated density. (**B**) apo-RF3 (and RF1) in RC-RF1•RF3 (L12-CTD not displayed) (**C**) RF3 in RC-RF3•GDPNP (***Gao et al., 2007***) (L12-CTD not shown). Superimposition (**D**) of closed conformation RF3•GDP (blue), semi-open apo-RF3 (green) and closed RF3•GTP (gray). Arrows indicate rotations of domain 3. (**E**) Close-ups of domain 3 conformations from (**A**)–(**D**). (**F**) Candidate residues in domain 3 of RF3 for a charge-based interaction with RF1 and 30S protein S12. (**G**) Candidate residues in RF1 helix α2 for a charge-based interaction with RF3. RF3 domains labeled in blue; α2 and α3 denote helices α2 and α3 in domain 1 of RF1. ***Figure 5—figure supplement 1*** shows superimposition of apo-RF3 and RF3•GDPNP.

DOI: 10.7554/eLife.00411.012

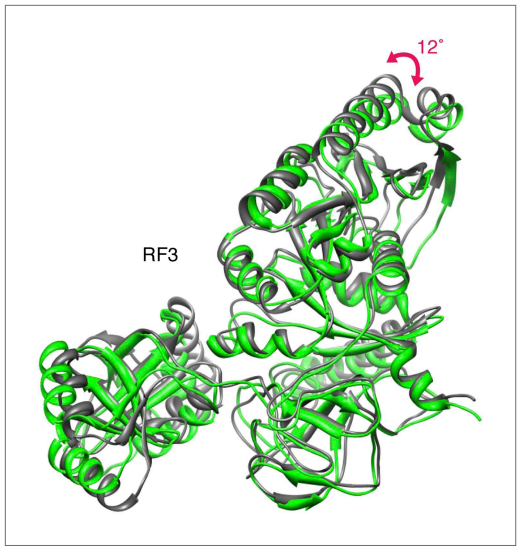


**Figure 5—figure supplement 1**. Movement of domain 1 in RF3. Superimposition of apo-RF3 (green) and RF3•GDPNP (gray). Domain 1 moves closer (arrow) to L6/SRL upon GDPNP recruitment to RF3 to mediate binding of RF3•GDPNP to L6/SRL.
DOI: 10.7554/eLife.00411.013

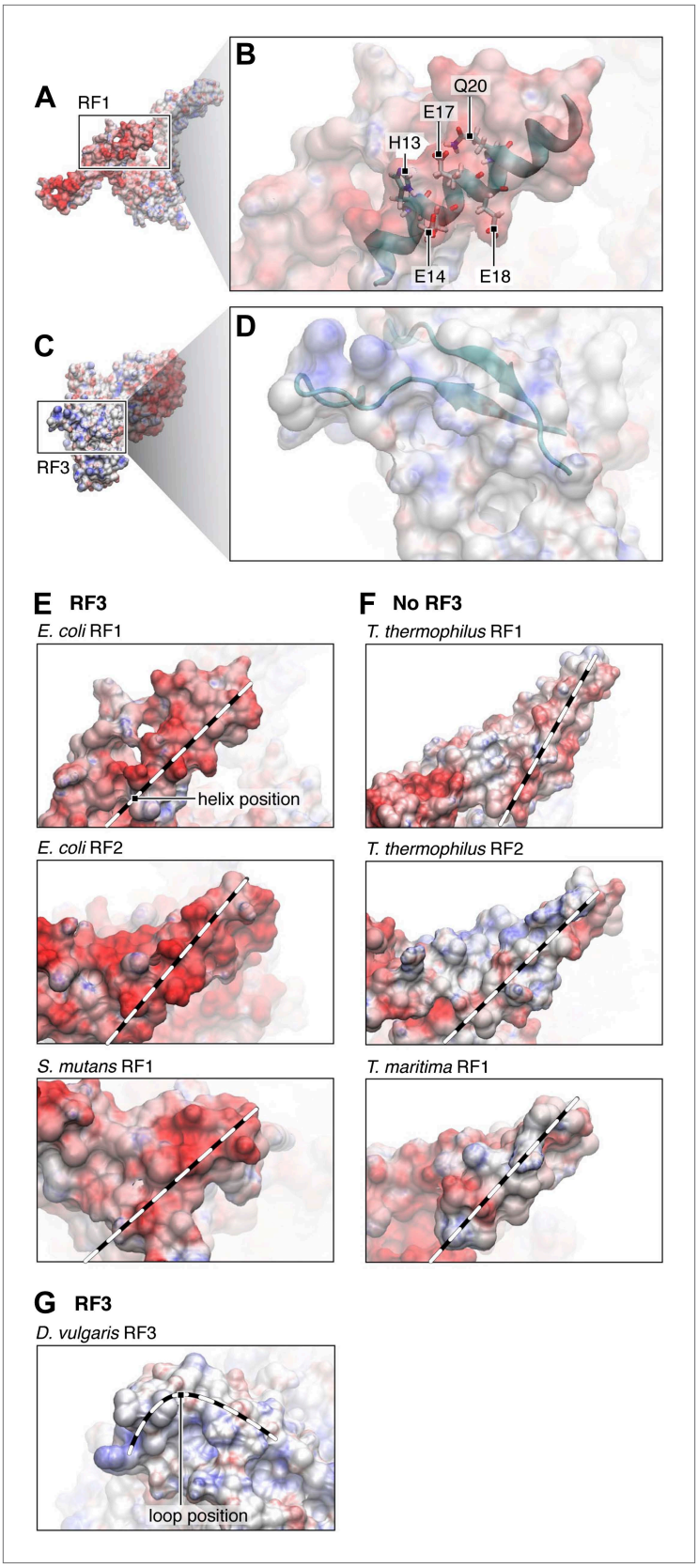


**Figure 6**. Electrostatic surface potentials of RF1 and RF3. (**A**) Electrostatic surface potential of RF1. Red surfaces are electronegative, blue surfaces electropositive. (**B**) Close-up of helix α2 in RF1, where interaction with RF3 is

*Figure 6. Continued on next page*

*Figure 6. Continued*

mediated. Labeled residues (pointers) are candidates (as identified by MDFF) for a direct interaction with RF3. The surface potential of helix α2 is electronegative. (**C**) Electrostatic surface potential of RF3. (**D**) Close-up of the two loops in domain 3 of RF3 posing charged or polar residues for contact with RF1. The surface potential of RF3 in this region is electropositive, pointing to a charge-based interaction between RF1 and RF3. In Bacteria expressing RF3 (**E**) the surface potential of RF1 in the α2 helical region (position of helix α2 indicated by dotted lines) is overall electronegative. In comparison, this region in class-1 RFs from Bacteria and Archaea not expressing RF3 (**F**) is overall electroneutral. (**G**) RF3 from *D. vulgaris* displays an electropositive surface similar to what we observe in *E. coli* RF3 (position of the flexible loop region indicated by dotted line). PDB IDs; *T. thermophilus* RF1: 3D5A, *T. thermophilus* RF2: 2WH3, *T. maritima* RF1: 1RQ0, *E. coli* RF1: current study, modeled/fitted from 2B3T, *E. coli* RF2: 1Gqe, *S. mutans* RF1: 1Zbt, *D. vulgaris* RF3: 3Vqt.

DOI: 10.7554/eLife.00411.014

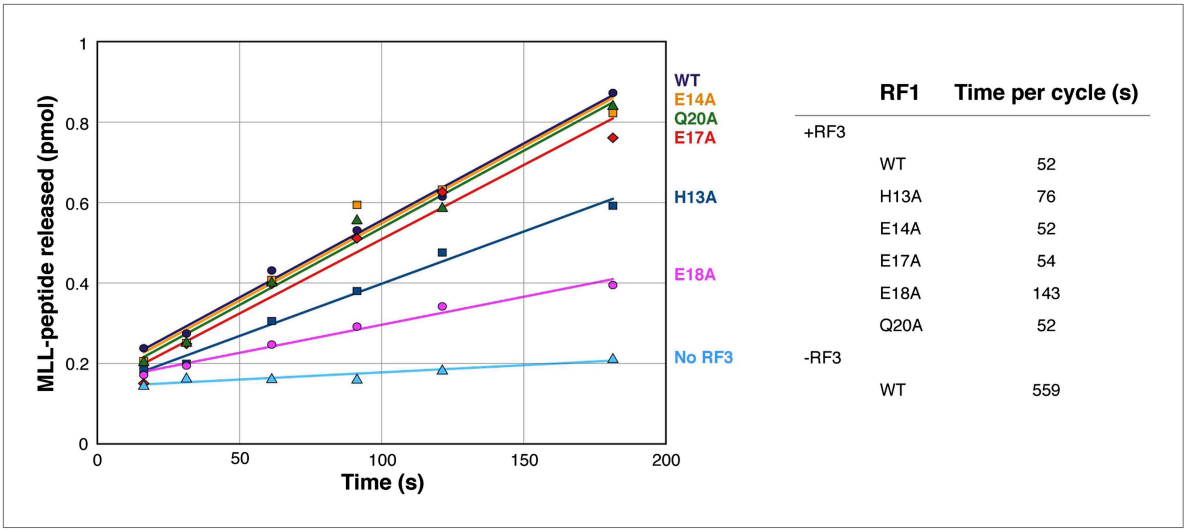


| | RF1 | Time per cycle (s) |
|---|---|---|
| +RF3 | | |
| | WT | 52 |
| | H13A | 76 |
| | E14A | 52 |
| | E17A | 54 |
| | E18A | 143 |
| | Q20A | 52 |
| -RF3 | | |
| | WT | 559 |

**Figure 7**. MLL release from RC due to RF3-mediated recycling of RF1 (WT and mutants). MLL release from RC due to recycling of RF1 WT and mutants with excess of RF3 over time. The chart shows recycling times for RF1 variants in the presence of RF3.

DOI: 10.7554/eLife.00411.015

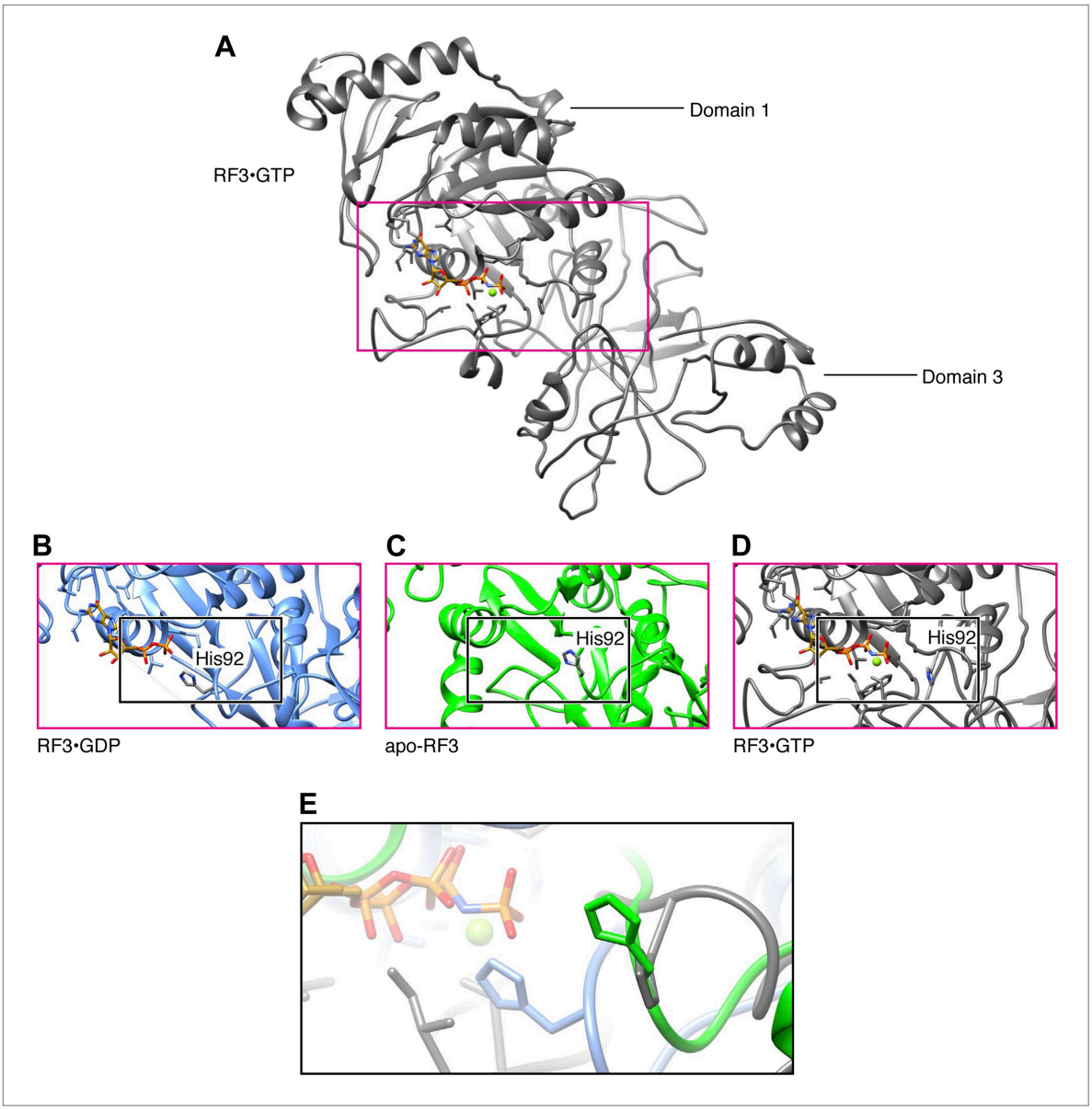


**Figure 8**. RF3 nucleotide loading-and-release. (**A**) RF3•GTP with the nucleotide-binding pocket inside the red box. (**B**)–(**D**) Nucleotide-binding pockets of RF3•GDP, apo-RF3 and RF3•GTP. In RF3•GDP, GDP is stabilized by interaction with H92. In apo-RF3 (**B**) and in RF3•GTP (**C**) H92 is retracted away from the nucleotide-binding pocket. Instead, this stabilization is performed by a $Mg^{2+}$ ion. (**E**) Superimposition of H92 position (black box in [**B**]–[**D**]) showing H92 in its GDP-stabilizing position (blue) and in its retracted positions (green and gray).

DOI: 10.7554/eLife.00411.016

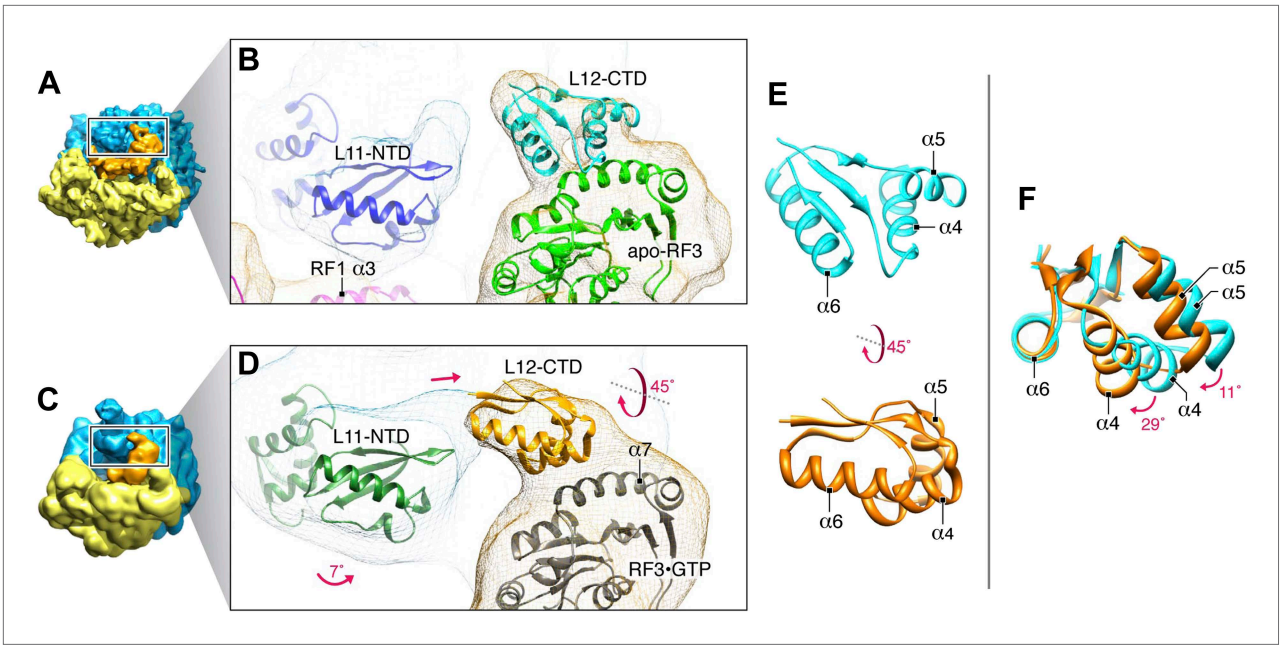


**Figure 9**. Dynamics of interactions involving RF3 and L12-CTD. (**A**) RC-RF1•RF3 map. (**B**) Close-up of RF1 helix α3, apo-RF3, L12-CTD and L11-NTD after fitting. (**C**) RC-RF3•GDPNP map (***Gao et al., 2007***). (**D**) Close-up of RF3•GDPNP, L12-CTD and L11-NTD after fitting. (**E**) L12-CTD position in (**B**) (cyan) and (**D**) (orange) displayed side-by-side. (**F**) Superimposition of L12-CTD from (**B**) and (**D**) showing the 'hinging-in' conformational change observed.

DOI: 10.7554/eLife.00411.017

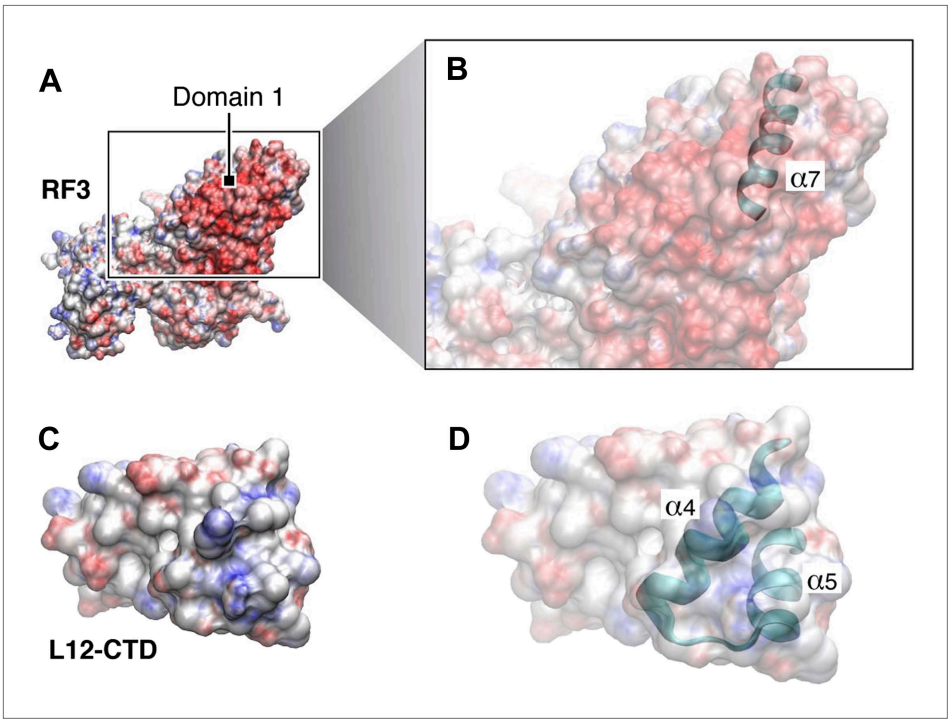


**Figure 10**. Electrostatic surface potentials of L12-CTD, RF3 and other major translational GTPases. Red surfaces are electronegative, blue surfaces electropositive. (**A**) The electrostatic surface potential of RF3 (**B**) Close-up of domain 1 in RF3, displaying the position of helix α7 in the G' subdomain responsible for binding to L12-CTD ([**C**]; close-up in [**D**]). The overall surface potential of the G' subdomain in RF3 is negative and the overall surface charge of helices α4 and α5 in L12-CTD is positive. ***Figure 10—figure supplement 1***: Surface potentials of IF2 (**A**) and (**B**), EF-Tu (**C**) and (**D**), and EF-G (**E**) and (**F**) are all electronegative in domain 1.

DOI: 10.7554/eLife.00411.018

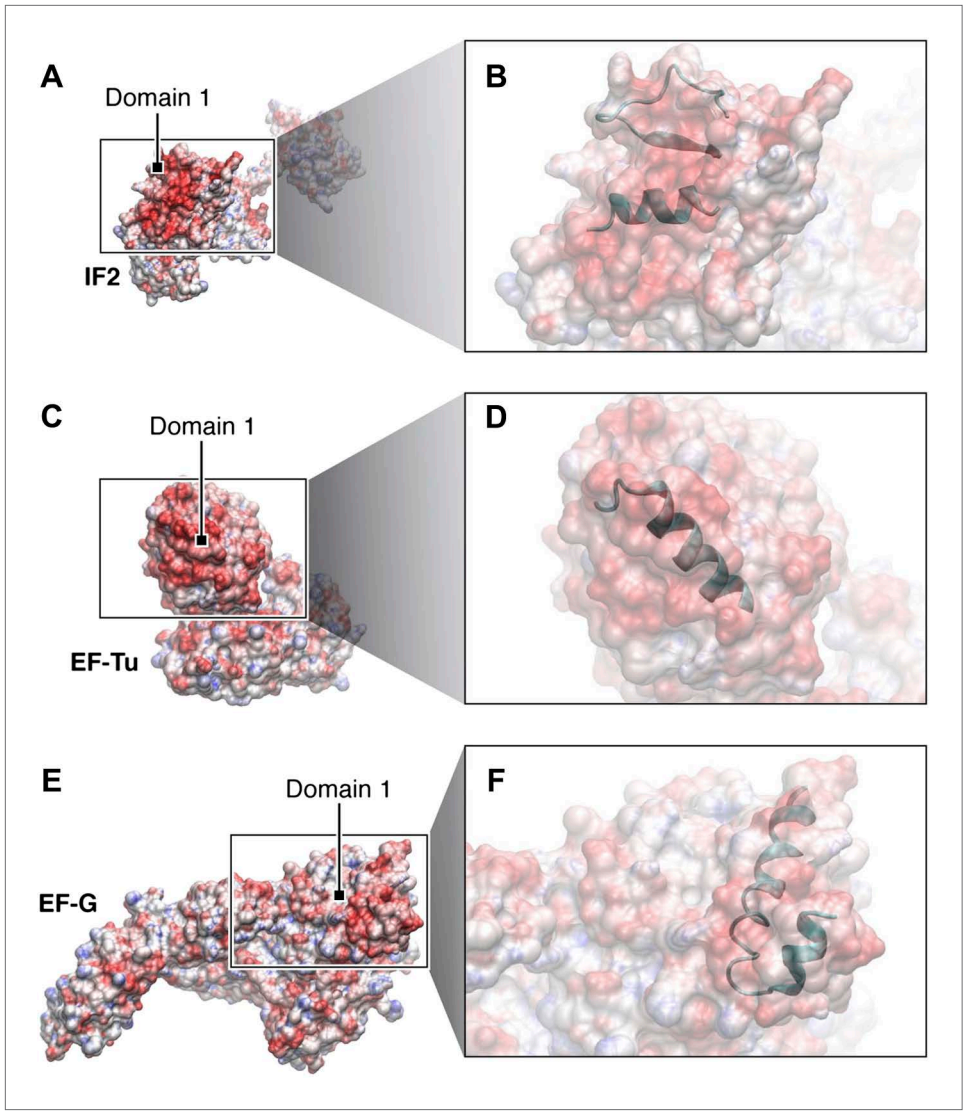


**Figure 10—figure supplement 1**. Surface potentials of IF1, EF-Tu and EF-G. Surface potentials of IF2 (**A**) and (**B**), EF-Tu (**C**) and (**D**), and EF-G (**E**) and (**F**) are all electronegative in domain 1, where they interact with the electropositive α4/α5 patch of L12-CTD. The close-ups display in ribbon the secondary structures involved in the interactions between L12-CTD and the major translational GTPases (***Kothe et al., 2004***; ***Allen et al., 2005***; ***Helgstrand et al., 2007***; ***Harms et al., 2008***; ***Gao et al., 2009***). PDB IDs are as follows: *E. coli* RF3: current study, modeled/fitted from 2H5E, *E. coli* L12-CTD: 1Ctf, *E. coli* IF2: 1ZO1, *E. coli* EF-Tu: 1DG1, *E. coli* EF-G: 2Wrk.
DOI: 10.7554/eLife.00411.019

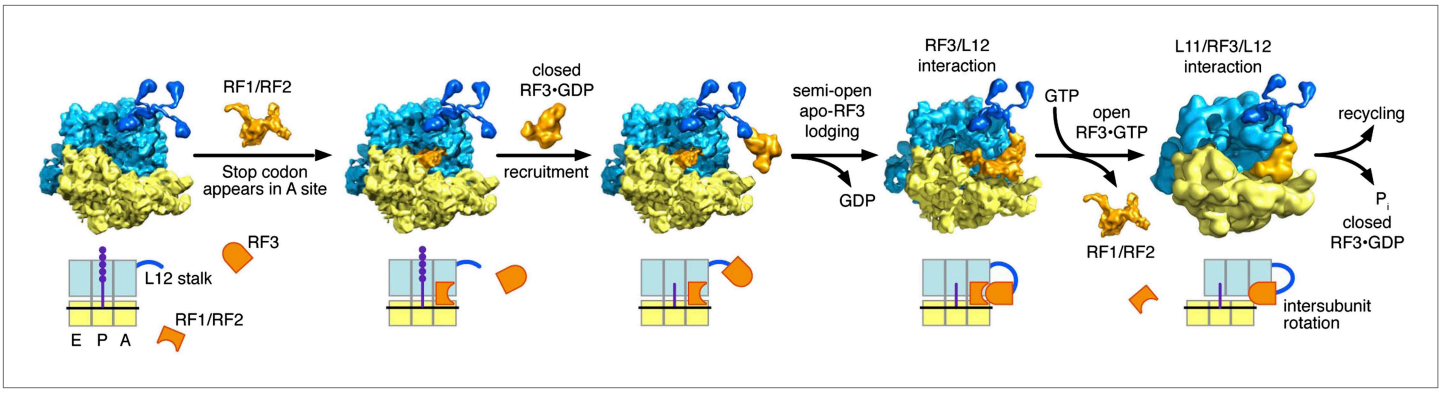


**Figure 11**. Proposed model of translation termination involving intersubunit-, L12-, RF1- and RF3-dynamics. A class-1 RF recognizes its cognate mRNA stop codon in the ribosome and binds in the A site. Here, the class-1 RF mediates release of the nascent protein attached to the P-site tRNA. After nascent protein release, RF3•GDP is recruited to the ribosome. RF3•GDP is in its closed form and does not form a stable complex with the ribosome; it is possible that initital contact between the ribosome and RF3•GDP is mediated by L12-CTD. As RF3 lodges onto the ribosome, GDP is released and apo-RF3 assumes its semi-open conformation. At this point, apo-RF3 is in contact with L12-CTD, the class-1 RF and 30S protein S12. Upon recruitment of GTP to apo-RF3, RF3•GTP assumes its open conformation and the ribosome changes from the unrotated macrostate I to the rotated macrostate II and the class-1 RF leaves the complex. In this state, RF3•GTP is in contact with L6/SRL and L12-CTD, already interacting with RF3, forms a bridge to L11-NTD. This binding state of RF3•GTP marks the onset of RF3's GTPase activity leading to cleavage of GTP and release of $P_i$. RF3•GDP dissociates from the ribosomal complex in its closed conformation and the ribosome is ready for subunit recycling.

DOI: 10.7554/eLife.00411.020